UC Berkeley
UC Berkeley Previously Published Works

Title

The Influence of Polymer Processing Methods on Polymer Film Physical Properties and Vascular Cell Responsiveness

Permalink

Journal

ACS Applied Bio Materials, 2(8)

ISSN

2576-6422

Authors

Ammann, Kaitlyn R
Li, Maxwell
Hossainy, Syed
et al.

Publication Date

2019-08-19

DOI

10.1021/acsabm.9b00175

Peer reviewed

The Influence of Polymer Processing Methods on Polymer Film Physical Properties and Vascular Cell Responsiveness

Kaitlyn R. Ammann[1], **Maxwell Li**[1], **Syed Hossainy**[2], **Marvin J. Slepian**[1,3,4,*]

[1]Department of Biomedical Engineering, College of Engineering, The University of Arizona, Tucson, AZ 85721, United States

[2]Department of Bioengineering, College of Engineering, The University of California Berkeley, Berkeley, CA, 94720

[3]Department of Medicine, College of Medicine, The University of Arizona, Tucson, AZ 85721, United States

[4]Sarver Heart Center, The University of Arizona, Tucson, AZ 85721, United States

Abstract

Implantable vascular devices typically interface with blood and vascular tissues. Physical properties of device materials and coatings, independent of chemical composition, can significantly influence cell responses and implant success. Here, we analyzed the effect of various polymer processing regimes, using a single implant polymer - poly(ε-caprolactone) (PCL), on vascular endothelial cell (EC), smooth muscle cell (SMC), and platelet response. PCL films were formed by varying three parameters: 1) formation method - solvent casting, melt pressing or spin coating; 2) molecular weight – 50 or 100 kDa; and 3) solvent type – dichloromethane (DCM) or tetrahydrofuran (THF). We quantified the relationship of polymer processing choice to surface roughness, wettability, and bulk stiffness; and to EC adhesion, SMC adhesion, and platelet activity state (PAS). Multiple regression analysis identified which processing method signficantly impacted (F-ratio>p-value; p<0.1) polymer physical properties and vascular cell interaction. Film formation method affected PCL roughness (R_q), wettability (°), and stiffness (MPa) with spin coating resulting in the most wettable (81.8±0.7°), and stiffest (1.12±0.07 MPa; p<0.001) polymer film; however, solvent cast films were the roughest (281±66nm). Molecular weight influenced wettability, with the highest wettability on 50 kDa films (79.7±0.7°; p<0.001) and DCM solvent films (83.0±1.0°; p<0.01). The multiple regression model confidently predicted (F-ratio=9.88; p=0.005) wettability from molecular weight (p=0.002) and film formation method (p=0.03); stiffness (F-ratio=4.21; p=0.05) also fit well to film formation method (p=0.02). Film formation method impacted SMC adhesion and platelet activity state, but not EC adhesion, with melt press PCL promoting the highest SMC adhesion (18000±1536 SMCs; p<0.05) and PAS (5.0±0.7

%PAS). The regression model confidently fit SMC adhesion (F-ratio=3.15; p=0.09) and PAS (F-ratio=5.30; p=0.05) to polymer processing choices, specifically film formation method (p<0.03). However, only SMC adhesion had a model that fit well (F-ratio=4.13; p=0.05) to the physical properties directly, specifically roughness and wettability (p<0.04).

Graphical Abstract
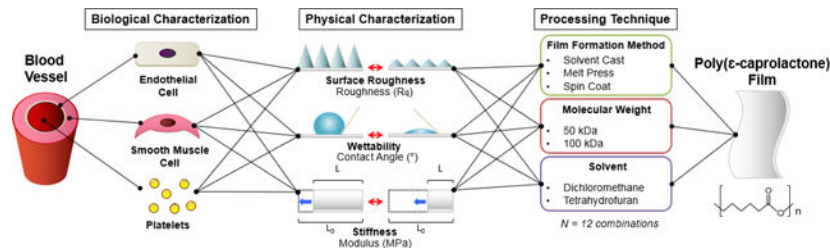
Keywords

biomaterials; polymer; tissue interaction; vascular; endothelial cell; smooth muscle cell; platelet

Introduction

Synthetic polymer films and coatings are utilized extensively for tissue engineering and fabrication of implantable medical devices[1]. Long-term implant success is dependent on the interaction of target site cells with biomaterial surfaces. In particular, interfacing surface topography, roughness, and hydrophilicity, as well as bulk mechanical stiffness of polymers are known to impact cell adhesion, migration, proliferation and differentiation of various cell types[2–5]. A particular domain of use of polymer-based implants are for treatment of cardiovascular diseases (CVD). CVDs are the leading cause of morbidity and mortality in the United States and the Western world[6]. Implantable devices such as stents, biodegradable scaffolds, endoluminal paving layers, stent grafts, ventricular assist devices and the total artificial heart have emerged as the mainstay of therapy for CVD, with their use continuing to increase[7–14]. While these devices significantly improve patient symptoms, hemodynamics and mortality, their interaction with vascular endothelial cells (ECs), smooth muscle cells (SMCs), and platelets can significantly impact their long-term efficacy and freedom from adverse events. A primary mechanism of dysfunction and failure of these devices is progressive vascular cell overgrowth with restenosis, or surface thrombosis with embolism, all leading to clinically significant events. Vascular cells dynamically respond to their environment, with particular sensitivity to the physical and biochemical properties of their substrates and surroundings[15].

SMCs are the dominant cell type that occupy the arterial media (middle layer), regulating blood pressure and blood flow distribution. In vascular injury or disease, SMCs migrate into and proliferate within the vessel lumen, forming a neointima, leading to progressive arterial obstruction[16–18]. Previous studies have revealed that SMCs, when subjected to a foreign implant material, respond more to stiffer versus softer substrates, with increasing migration and adhesion on materials with moduli up to hundreds of kPa[19,20].

Endothelial cells compose the blood-contacting luminal layer and are essential in maintaining vessel wall homeostasis as well as surface thromboresistance[21–24]. EC adhesion, proliferation, and migration behavior are vital in maintaining this anti-thrombotic, blood-contacting surface. With regard to implant material response, ECs demonstrate similar behavior to SMCs, preferring adhesion to rougher, stiffer materials, similar to surrounding ECM stiffness in the kPa to MPa range; and hydrophilic surfaces with contact angle up to 100° at the liquid-substrate-air interface [25–27].

Platelets are vital cellular elements in blood, critical to the maintenance of vascular hemostasis, preventing bleeding in vascular injury, rapidly responsive to biochemical and mechanical stimuli. In the case of disease or exposure to foreign materials, platelets adversely form thrombi contributing to pathologic vascular occlusion[28]. Prior studies have shown that substrate surface properties are critical determinants of platelet responsiveness and activation. Specifically, increasing surface roughness especially under flow can lead to shear-mediated platelet activation and thrombosis[29]. Additionally, higher hydrophilicity can increase platelet interaction and subsequent activation at the biomaterial surface[30].

To optimize vascular implant hemocompatibility, fabrication strategies aimed at promoting EC adhesion while simultaneously limiting SMC adhesion and platelet activation would improve device efficacy and safety. It is therefore beneficial to define optimal properties of biomaterials that differentially impact these vascular cells. While studies have focused on the utility of nano- and micro-texturing to design biomaterial surfaces and influence cell interactions, many of these methods are time-consuming, expensive, non-transferable to manufacture and unrealistic for application to implantable devices[31]. In contrast, in the present study we first examine the effect of basic polymer processing methods on the physical properties of films formed using a prototypic cardiovascular implant polymer - poly(ε-caprolactone) (PCL). We specifically focused on exploring the influence of: 1) formation method - solvent casting, melt pressing or spin coating; 2) molecular weight – 50 or 100 kDa; and 3) solvent type – dichloromethane (DCM) or tetrahydrofuran (THF). We examined the impact of polymer processing choice and physical properties generated on EC adhesion, SMC adhesion, and platelet activation state. We hypothesized that interfacing polymer properties generated would influence vascular cell activity; and that this relationship is quantifiable and can be utilized to inform optimal PCL processing choices.

Experimental

Polycaprolactone film formation.

PCL pellets, 50 kDa (26289 Polysciences Inc., Warrington, PA, USA) or 100 kDa (1031 Scientific Polymer Products Inc., Ontario, NY, USA), were dissolved in either tetrahydrofuran (THF; 3404 Honeywell Burdick & Jackson, Muskegon, MI, USA) or dichloromethane (DCM; 4944531L Honeywell Burdick & Jackson, Muskegon, MI, USA) (5% w/v). To ensure complete dissolution, solutions were stirred for 24 hours at room temperature prior to further processing.

Solvent casting.—Ten mL of PCL solution (5% w/v) was poured into 9 x 11 cm stainless steel pans and allowed to spread for uniform distribution. Pans were covered and allowed to

vent for 12 hours in a chemical fume hood. Only the evaporating polymer surface was used for cell experimentation. Schematic of solvent casting is shown in Figure 1A.

Melt pressing.—Solvent cast films were centered between mirror-polished stainless steel 7 x 7 in. platens (S416–8 MetalsDepot, Winchester, KY, USA). Films were pressed between these platens at approximately 102 psi (5000 lbf) and then heated to 70 °C with a Carver benchtop hydraulic press (3851–0 Carver Inc., Wabash, IN, USA). Once 70 °C was reached and PCL film samples were fully melted, heating was terminated, and films were allowed to cool to room temperature for 12 hours, followed by pressure release. Schematic of solvent casting is shown in Figure 1B.

Spin coating.—Three mL of PCL solution (5% w/v) was deposited onto the center of a clean glass microscope slide mounted on a chuck of a spin coater system (PWM32 Headway Research Inc., Garland, TX, USA). The slide was spun at 50 rpm for 15 seconds, followed by 100 seconds of variant speed (500–600 rpm) depending on PCL molecular weight and solvent, then 1500 rpm for 100 seconds. To achieve desired film thickness, an additional 3 mL of solution was immediately deposited onto the polymer slide and the process was repeated. Schematic of solvent casting is shown in Figure 1C.

PCL film post-processing.—After processing, all films were vacuum dried at 37 °C for 24 hours to ensure complete solvent evaporation. Films were created such that thickness was 70 ± 10 μm and measured using an electronic micrometer (IP54 Swiss Precision Electronics Inc., La Palma, CA, USA.) before further characterization. Prior to work with cells, films were rinsed thrice with DI water, once with ethanol (E7023 Sigma-Aldrich, St. Louis, MO, USA), and once with DI water. The samples were then UV treated for 15 min.

Film topography characterization.

PCL films were cut into 0.25 cm x 0.25 cm squares and mounted to glass cover slips. Surface topography was imaged using an atomic force microscope (AFM; MultiMode 8 Bruker Nano Surface, Santa Barbara, CA, USA) in tapping mode (625 μm^2 scan size, 512 samples/line, 0.8 Hz scan rate). Roughness characterization was completed in triplicate for each PCL film type, and root mean square roughness (R_q) were determined utilizing the Bruker Nanoscope Analysis software (V1.40 Bruker Nano Surface, Santa Barbara, CA, USA) with the integrated roughness tools. Before roughness quantitation, surface images were plane fitted (1st order) and flattened (1st order) to prevent sample bowing or tilting from affecting topography parameters. The digital approximation of R_q utilized by the software is as shown[32]:

$$R_q = \sqrt{\frac{Z_1^2 + Z_2^2 + \dots Z_N^2}{N}}$$

Z = profile height values

N = number of data points

Film wettability characterization.

Controlled characterization of hydrophobicity of PCL films was accomplished with a contact angle goniometer (CAM100 Raymarine Inc., Nashua, NH, USA). Ten μL drops of nano-pure water were added onto the film surface and imaged over 6 seconds, at 2 second intervals. Mean contact angle was calculated by obtaining the average of the left and right contact angles. Wettability characterization was repeated in triplicate for each PCL film type. Young's equation for contact angle is as shown[33]:

$$Y_S = Y_L \cdot cos(\theta) + Y_{SL}$$

Y_S = solid surface tension

Y_L = liquid surface tension

Y_{SL} = solid-liquid boundary tension

Film stiffness characterization.

Stiffness of PCL films were characterized in triplicate using a dynamic mechanical analyzer (RSA-G2 TA Instruments, New Castle, DE, USA) in tensile mode. PCL samples of equal length and width were strained at room temperature at a rate of 500 μm/s until fracture. Stiffness was calculated from force and strain data using the Young's modulus formula[34]:

$$E = \frac{F * L_0}{A * \Delta L}$$

E = Young's modulus

F = force exerted

A = cross-sectional area

L0 = initial length of polymer

L = change in length

Cell culturing.

Primary human umbilical vein endothelial cells (HUVECs; C-12200 PromoCell GmbH, Heidelberg, DEU) and primary human umbilical artery smooth muscle cells (HUASMCs; C-12500 PromoCell GmbH, Heidelberg, DEU), were used to assess vascular cell adhesion onto the PCL film samples. HUVECs were cultured in endothelial cell growth medium (C-22011 PromoCell GmbH, Heidelberg, DEU) supplemented with 1% (v/v) penicillin-streptomycin, 2% (v/v) fetal bovine serum, 0.4% (v/v) endothelial cell growth supplement, 0.1 ng/ml EGF, 1 ng/ml bFGF, 90 μg/ml heparin, and 1 μg/ml hydrocortisone. HUASMCs were cultured in smooth muscle cell growth medium (C-22062 PromoCell GmbH, Heidelberg, DEU) supplemented with 1% (v/v) antibiotic-antimycotic, 5% (v/v) fetal bovine serum, 0.5 ng/ml EGF, 2 ng/ml bFGF, and 5 μg/ml insulin. All cells were incubated at 37 °C,

5% CO_2 and grown to 80% confluency before use with experiments. Only passages between 3 and 6 were used for both cell lines.

Cell adhesion quantification.

Cell adhesion to (1 x 1 cm) PCL films was measured by fluorescence-based assay, CyQUANT® Cell Proliferation Kit (C7026 Invitrogen, Carlsbad, CA, USA). In brief, Pyrex® cylinders (31666 Corning Inc., Corning, NY, USA) were placed on top of each film in a 24-well plate to provide a barrier in which 50 μL of cells (1 x 10^5 cells/mL) were deposited into and allowed to seed for 4 hours at 37 °C, 5% CO_2. Cylinders were then removed, 450 μL cell media was added and plates were incubated for additional 20 hours. After 24 hours (total adhesion time), media was aspirated from wells, and PCL surfaces were gently rinsed with 1X phosphate-buffered saline (PBS; 10010023 Thermo Fisher Scientific, Carlsbad, CA, USA). The cells were frozen at −80 °C. After 24 hours, plates were thawed at room temperature; 200 μL of diluted CyQUANT® fluorescent dye was added and incubated at room temperature for 5 minutes. Fluorescence was measured with a spectrophotometric plate reader (FilterMax F5 Molecular Devices, San Jose, CA, USA) with filters at 480 nm excitation and 520 nm emission maxima.

Blood preparation and platelet isolation.

Blood was obtained from human donors, following informed consent, via venipuncture, mixed with 10% (v/v) acid citrate dextrose (ACD-A) and then centrifuged at 350 x g for 15 minutes. Platelet-rich plasma (PRP) from the top layer of centrifuged blood was filtered through a gel filtration column packed with Sepharose 2B beads (1701300 GE Healthcare Life Sciences, Chicago, IL, USA). Gel-filtered platelets (GFP) were collected from the column and counted using a particle counter (Dual Z1 Beckman Coulter, Brea, CA, USA). All experiments were performed at a GFP concentration of 20,000 platelets/μL; dilutions were done using a HEPES-modified Tyrode's buffer (i.e. "platelet buffer") with 3 mM $CaCl_2$ added 10 minutes prior to experimentation.

Platelet adhesion and activation.

The platelet activity state (PAS) assay quantifies real-time platelet activation and thrombin generation rate[35]. GFP samples (1 ml) were incubated at room temperature with individual PCL films for 30 minutes. After 30 minutes incubation, GFP were aspirated at the surface of each PCL film and assessed for their platelet activity state. Tissue culture treated plates were used as a positive control. Thrombin generation was quantified using spectrophotometric plate reader (VersaMax Molecular Devices, San Jose, CA, USA) measuring absorbance at 405 nm over 7 minutes. Chromozym-TH (11585398 Roche Diagnostics GmbH, Mannheim, DEU) was used as a thrombin-specific chromogenic peptide substrate. Thrombin generation rate was quantified as linear fit of absorbance over time and displayed as PAS value. This value was normalized to the thrombin generation rate of GFP sample sonicated with a digitial sonifier (SLPt Branson Ultrasonics, Danbury, CT, USA)to yield a PAS percentage.

Statistical analysis.

PCL film experiments were executed in triplicate or more for physical characterization of surfaces; biological characterization experiments were performed $n = 9$ times. Data were analyzed by Welch's unpaired t-test or ANOVA with unequal variances. P-values < 0.05 values were considered statistically significant. To consider all factors characterized, multiple regression analysis was performed using standard least squares method with JMP software (V14 SAS Institute Inc., Cary, NC, USA). The regression model was assessed for collinearity or confounding variables by assessing correlation between residuals of variables. The model was a good fit with p-value < 0.05 and F-ratio of overall significance higher than the p-value. A regression model from the predictors was formed using significant parameter estimates (p < 0.05) as coefficients for the corresponding dependent variables; insignificant parameter estimates were discarded from the model.

Results

Uniform PCL film creation and validation.

Twelve unique PCL films were successfully fabricated by varying solvent (DCM, THF), molecular weight (50 kDa, 100 kDa), and film formation method (solvent cast, melt press, spin coat) (Figure 1). All films were verified to have consistent thickness (70 ± 10 um) prior to further characterization. To verify film purity and complete solvent evaporation, differential scanning calorimetry (DSC) was additionally performed (representative DSC graph in Figure S1). DSC analysis confirmed the identity of the PCL films, with melting temperatures at approximately 60 °C and crystallinity temperature at approximately 28 °C. During preliminary qualitative analysis, each polymer process was found to yield qualitatively distinct surface topography and roughness, as seen in the captured brightfield and atomic force microscopy (AFM) images (Figure 2); further supporting scanning electron microscope (SEM) images are shown in Figure S2.

Physical characterization of films.

Roughness.—To quantify surface topography of each PCL film surface, roughness values (R_q) were derived from AFM data and were found to range between 46 nm (solvent cast, DCM, 100 kDa) to 755 nm (solvent cast, THF, 100 kDa). Interestingly, the most and least rough films were both solvent cast 100 kDa PCL films, emphasizing the contributory effect of solvent on surface roughness (Figure 3A). Additionally, melt press films were consistently smooth regardless of solvent or molecular weight, likely due to being processed on mirror-polished stainless steel. When considering film formation method alone, solvent cast films were rougher than spin coat and melt press (p < 0.01) films (Figure 3B). Trends also identified that PCL films made with 100 kDa molecular weight or THF solvent were rougher, though this difference was not strictly statistically significant (Figure 3C and Figure 3D).

Wettability.—Hydrophilicity of the PCL films were examined by contact angle analysis with deionized water. Contact angle measurements ranged from 69.8° (melt press, DCM, 50 kDa) to 104.1° (solvent cast, THF, 100k Da) (Figure 4A). In this case, higher contact angle corresponds to lower hydrophilicity or wettability of the PCL film. The trend between film

formation methods was relatively consistent, with solvent cast films being the least hydrophilic, with a significantly higher contact angle than melt press or spin coat films ($p < 0.001$) (Figure 4B). Similarly, the trend among molecular weight and solvent choice was consistent, leading to a significantly higher contact angle for 100 kDa PCL ($p < 0.001$) and THF solvents ($p < 0.01$) (Figure 4C and Figure 4D). From this data, we can conclude that spin coat, 50 kDa, DCM films had highest wettability; solvent cast, 100 kDa, THF films had lowest wettability.

Stiffness.—Differential mechanical analysis (DMA) was used to obtain tensional stress versus strain of each PCL film to determine its bulk stiffness (Young's modulus). Measured PCL bulk stiffness ranged from 0.59 MPa (solvent cast, THF, 100 kDa) to 1.75 MPa (spin coat, THF, 100 kDa); similar to independent examinations of PCL tensile modulus[36] (Figure 5A). Interestingly, both the least and most stiff films were formed with THF and 100 kDa PCL, emphasizing the effect of film formation method on bulk polymer stiffness. This effect is seen when considering film formation method alone; spin coat films were significantly stiffer than solvent cast ($p < 0.001$) and melt press ($p < 0.001$) films (Figure 5B). In contrast, there was no significant difference in stiffness when considering only molecular weight or solvent choice (Figure 5C and Figure 5D).

Biological characterization of films.

EC adhesion.—Approximately 5,000 human umbilical vein endothelial cells (HUVECs) in media were seeded on each PCL film for 24 hours. The number of adherent endothelial cells (ECs) on the surface of the polymer sample (1 x 1 cm) after 24 hours ranged between 871 ECs (solvent cast, DCM, 50 kDa) to 38,007 ECs (solvent cast, THF, 50 kDa) (Figure 6A). Because the highest and lowest adhesion occurred on solvent cast 50 kDa films, PCL solvent choice could impact EC adhesion. However, EC adhesion was highly varied, contributing to the lack of a significant difference in EC adhesion found between film formation method, molecular weight, or solvent choice (Figure 6B, Figure 6C, and Figure 6D). In fact, while EC adhesion was significantly higher on solvent cast DCM 100 kDa films, compared to DCM 50 kDa films, the opposite effect was seen on spin coat films with the same solvent and molecular weights, suggesting there could be a significant confounding factor influencing EC adhesion. On average, all films supported EC viability and growth during the 24-hour culture period. Fold-increase of cell count is shown in Table S1.

SMC adhesion.—Approximately 5,000 human umbilical artery smooth muscle cells (HUASMCs) in media were seeded on each PCL film for 24 hours. The number of adherent smooth muscle cells (SMCs) on the surface of the polymer sample (1 x 1 cm) after 24 hours ranged between 2,285 SMCs (melt press, THF, 100 kDa) and 71,059 SMCs (spin coat, DCM, THF) (Figure 7A). Unlike with EC adhesion, the SMC adhesion differences between film formation methods were significant. Spin coat films adhered more SMCs than solvent cast ($p < 0.05$) or melt press ($p < 0.001$) films. Solvent cast films also adhered significantly more SMCs than melt press ($p < 0.005$) films (Figure 7B). Like ECs, SMC adhesion was not significantly different between molecular weight or solvent choices, however, the trend revealed higher adhesion with 100 kDa molecular weight and DCM solvent, opposite to the (non-significant) trends seen with EC adhesion (Figure 7C and Figure 7D). On average, all

films supported SMC viability and growth during the 24-hour culture period. Fold-increase of cell count is shown in Table S2.

Platelet activation.—One mL of gel-filtered platelets (GFP) (20,000 platelets/μL) were incubated for 30 minutes on the PCL films. Activation of platelets after PCL surface exposure were analyzed via colorimetric assay and normalized to a positive sonicated control. In this case, platelet activation is the precursor for blood clotting, and a higher platelet activity state (PAS) translates to a higher likelihood of thrombus formation at the blood-material interface. The measured PAS on each PCL film ranged from 0.8% (spin coat, DCM, 50 kDa) to 15.5% (melt press, DCM, 100 kDa) (Figure 8A). Additionally, there were differences among the different film formation methods, however, these were not statistically significant. Melt press films had higher platelet activation than both spin coat and solvent cast (p = 0.05) films (Figure 8B). In contrast, molecular weight and solvent choice were similar in their effects on PAS (Figure 8C and Figure 8D). Qualitative SEM images of platelets adhered to the PCL film surfaces are shown in Figure S2.

Effects of polymer processing choices on physical characteristics.

Multiple regression modeling using a standard least squares method was performed with the data collected from the PCL films to assess the effect of film formation method, solvent, and molecular weight on the measured roughness, wettability and stiffness of each film. With this regression model, input factors (polymer processing choice) could potentially predict response (physical properties) of the PCL film. Table 1 depicts the outputs from the model with statistically significant model fits and independent variables denoted by italicized values.

Interestingly, roughness did not have a significant model fit, however, wettability and stiffness fit well with the regression model when considering film formation method or molecular weight. Specifically, wettability could be predicted by molecular weight choice or film formation method. Equation 1 displays the regression model with these significant parameters inputted, all other factors were deemed negligible. Unlike wettability, stiffness was only significantly impacted by film formation method and was a less significant fit to this model. Equation 2 shows the relationship between film stiffness and film formation choice.

Equation 1. Wettability Regression Model by Molecular Weight and Film Formation Method

$$Contact\ Angle = 84.90 + 5.31(MW50) - 5.31(MW100) + 5.27(FSVC) - 2.34(FMP) + -2.93Xe(FSPC)$$

Where MW50 and MW100 correspond to PCL molecular weight of 50 kDa and 100 kDa, respectively; FSVC, FMP, and FSPC correspond to PCL formation method of solvent cast, melt press, or spin coat, respectively. With this categorical model, the parameter equals 1 if the PCL film is formed with that molecular weight or that formation method; otherwise parameter is 0 (e.g. MW50=1, MW100=0; FSVC=1, FSMP=0, FSPC=0 for a 50 kDa, solvent cast PCL film).

Equation 2. Stiffness Regression Model by Film Formation Method

$$Stiffness = 0.87 - 0.10(FSVC) - 0.15(FMP) + 0.25(FSPC)$$

Where variables correspond to same parameters described for Equation 1.

Effects of physical characteristics and polymer processing choices on biocompatibility.

PCL film wettability, stiffness, and roughness data were fit to a regression model with biological characteristics as the dependent variables to examine the impact of each polymer physical property on cell interaction. Table 2 shows the statistical outputs from our model fitting. PAS and EC adhesion did not fit well to any linear multiple regression model with these independent variables. However, SMC adhesion had a significant relationship with PCL roughness and stiffness. Although less statistically significant than roughness, it is interesting to note that the stiffness had a very large impact on SMC adhesion compared to roughness, which can be seen with the much higher parameter estimate value. Equation 3 depicts the relationship between roughness, stiffness and SMC adhesion.

Equation 3. SMC Adhesion Regression Model by Roughness and Stiffness

$$SMC\ Count = 33024.26 + 57.82(RQ) + 36901.30(YM)$$

Where RQ corresponds to the measured roughness (R_q) of the PCL film in nm and YM corresponds to the measured Young's Modulus (bulk stiffness) of the PCL film in MPa.

PCL film formation method, molecular weight, and solvent choices data were similarly fit to a regression model with biological characteristics as the dependent variables to see the impact of each polymer decision on vascular cell interaction. Table 3 shows the outputs from the multiple regression model in which SMC adhesion and PAS each fit well to film formation method, while EC adhesion did not fit will to any of the described independent variables. Specifically, melt press films significantly decreased SMC adhesion while significantly increasing PAS, as seen from the high parameter estimates. Equations 4 and 5 depict this mathematical relationship to SMC adhesion and PAS, respectively.

Equation 4. SMC Adhesion Regression Model by Film Formation Method

$$SMC\ Count = 29746.28 + 1588.17(FSVC) - 11746.64(FMP) + 10158.47(FSPC)$$

Where variables correspond to same parameters described for Equation 1.

Equation 5. PAS Regression Model by Film Formation Method

$$Platelet\ Activity\ State = 0.04 - 0.011(FSVC) + 0.008(FSMP) + 0.003(FSPC)$$

Where variables correspond to same parameters described for Equation 1.

Discussion

In this study, we go beyond simply identifying polymer processes that yield high cell adhesion by quantifying the differential interaction of vascular cells as they relate to multiple polymer processing states and resultant physical characteristics. Despite use of PCL films that are chemically identical, we found that specific, individual physical properties, influenced by polymer processing techniques, significantly impacted cell interaction. However, not all measured properties had confidently quantifiable relationships to cell behavior. EC adhesion specifically, was not significantly impacted by any of the polymer processing variations; whereas SMC adhesion and PAS differed, depending on the film formation method employed. Similarly, roughness, wettability, and stiffness were all significantly different when film formation method changed; however only wettability changed due to solvent or molecular weight variations.

The native vasculature is a complex, multi-layered tissue composed of a variety of different cells and matrix proteins, all of which individually play an integral role in the healthy behavior of surrounding cells and tissue. So too, then, should be the level of complexity considered when choosing polymer processing methods for implantable polymers that are bolstering or replacing the native extracellular matrix (ECM) of the arterial wall. While the relationship between cells and their environments are too complicated to be modeled by a single linear equation, isolating influencing factors and subsequent cell responses in this study has provided insight into the impact of individual factors on cell-specific behavior for potential vascular applications. As our results indicate, ECs do not seem to be as impacted by physical cues as SMCs and platelets; previous studies have indicated however, that they respond strongly to chemical interaction with integrins and extracellular matrix[37,38]. EC adhesive behavior could be more dependent on a biochemical interaction with the surface over a physical interaction, as suggested by some previous studies[39–41]. Therefore, it may be important to consider both biochemical factors (i.e. ECM coating) to enhance EC adhesion while simultaneously tuning physical properties that reduce SMC adhesion and PAS when making biomaterial choices. Accounting for the lowest SMC adhesion and PAS, our results indicate that melt pressed PCL films formed with THF would be the best option. While molecular weight caused wettability to change (50 kDa higher wettability, lower surface contact angle), the effect on vascular behavior was inconclusive with no significant change in PAS, SMC, or EC adhesion. Despite this, molecular weight was a significantly impactful parameter for determining wettability in our multiple regression model.

The differences between the significant cell response to physical parameters versus "goodness-of-fit" to our model are likely due to either confounding factors not considered here, or a nonlinear relationship within the ranges for the parameters studied.[42,43] Parameters for describing surface roughness, specifically, are commonly scrutinized for their ability to accurately describe surface micro- and nano-architecture; in response to this, some studies have examined effects of alternative roughness parameters such as surface skewness, kurtosis, surface area increase, and surface peak counts.[44–47] Skewness and kurtosis especially have been investigated as they relate to osseointegration of bone implants with osteoblasts or osteoclasts, but have widely been ignored in the field of cardiovascular biology and vascular tissue-polymer interactions.[48–50] In brief, skewness describes the bias

of the roughness profile in relation to the average roughness whereas kurtosis describes the sharpness of the surface topography. To investigate possibility of improved model fit with alternative roughness parameters we analyzed surface skewness and kurtosis and their relationship to vascular behavior and polymer processing choices. Only skewness had a significant relationship with film formation method, which further translated to significant impact on PAS (information in Supplementary Materials; Table S3 and S4, Equation S1 and S2). This emphasizes the point that roughness from topographic amplitude alone cannot accurately define the relationship between surface interaction, but rather the shape and slopes of peaks in which cells, especially platelets, interact can impact behavior. This could potentially be the case for describing wettability and mechanical properties of polymers as well. While the skewness data here matched well to PAS, the surface roughness only described a 25 by 25 um^2 area of PCL; previous studies have shown that scaling the surface area probed for roughness to match the size of the cell or tissue in question could potentially translate better to larger cell types like endothelial and smooth muscle cells.[51–53] Multi-scale modeling of roughness versus vascular cell behavior is an avenue we plan to explore in future work in addition to investigating a wider variety of roughness, wettability and mechanical parameters of the polymers. Application to a variety of cardiovascular-relevant polymers not discussed here will additionally be explored; of particular interest are a range of co-polymers used in device coatings (PLGA, PLLA), polyurethanes used in scaffolds, and fluoropolymers used in grafts and suture sealing (PTFE)[54–56].

Study Limitations.

The vascular system is a complex environment difficult to simulate in *in vitro* experimentation. For accurate representation of the lumen-vessel interface, dynamic conditions including the 3-D extracellular environment, non-Newtonian flow, and hydrostatic pressure should be considered. Although cell adhesion or activation was explored here, this is a precursor to other, subsequent important cell responses which may provide more information about long-term cell integration. Future studies examining cell morphology, spreading, migration, proliferation, and phenotypic differentiation would be a valuable and potentially provide additional conclusions from adhesion alone. These *in vitro* studies did not consider the competitive nature of adhesion to a surface in which many proteins and cell types are competitively interacting to take up space on a surface. Instead, we chose to isolate our variables to see the interaction of single biologic components.

Conclusions

How polymers are physically fabricated matters. In the case of polymer implants or medical device coatings, even the smallest of changes in film formation method, molecular weight, and solvent can impact how cells interface with the implant or device. From this study we find that film formation especially is important for informing cell response in vascular SMCs and platelets, with melt press PCL formed with THF solvent resulting in the desired minimal adhesion. Despite all factors studied not providing a simple defined relationship, we can use many of the polymer processing methods and resultant physical properties to inform choices as to how to create PCL films for vascular-related medical implants. With further work, this model may be enhanced, allowing consideration of additional parameters to increase its

Author Manuscript

accuracy of representing and predicting vascular cell-biomaterial interactions at the implant polymer interface.

Supplementary Material

Refer to Web version on PubMed Central for supplementary material.

Acknowledgments

References

(1). Teo AJT; Mishra A; Park I; Kim Y-J; Park W-T; Yoon Y-J Polymeric Biomaterials for Medical Implants and Devices. ACS Biomater. Sci. Eng 2016, 2 (4), 454–472.

(2). Alves NM; Pashkuleva I; Reis RL; Mano JF Controlling Cell Behavior Through the Design of Polymer Surfaces. Small 2010, 6 (20), 2208–2220. [PubMed: 20848593]

(3). Sanz-Herrera JA; Reina-Romo E. Cell-Biomaterial Mechanical Interaction in the Framework of Tissue Engineering: Insights, Computational Modeling and Perspectives. Int. J. Mol. Sci 2011, 12 (11), 8217–8244. [PubMed: 22174660]

(4). Discher DE; Janmey P; Wang Y. Tissue Cells Feel and Respond to the Stiffness of Their Substrate. Science (80-.). 2005, 310 (5751), 1139–1143.

(5). Wang D; Liu M; Gu S; Zhou Y; Li S. Microtopography Attenuates Endothelial Cell Proliferation by Regulating MicroRNAs. J. Biomater. Nanobiotechnol 2017, 8, 189–201.

(6). Benjamin EJ; Virani SS; Callaway CW; Chamberlain AM; Chang AR; Cheng S; Chiuve SE; Cushman M; Delling FN; Deo R; et al. Heart Disease and Stroke Statistics—2018 Update: A Report From the American Heart Association. Circulation 2018, 137 (12), e67–e492. [PubMed: 29386200]

(7). McMahon S; Bertollo N; Cearbhaill EDO; Salber J; Pierucci L; Duffy P; Dürig T; Bi V; Wang W. Bio-Resorbable Polymer Stents: A Review of Material Progress and Prospects. Prog. Polym. Sci 2018, 83, 79–96.

(8). Im SH; Jung Y; Kim SH Current Status and Future Direction of Biodegradable Metallic and Polymeric Vascular Scaffolds for Next-Generation Stents. Acta Biomater. 2017, 60 (15), 3–22. [PubMed: 28716610]

(9). Slepian MJ Polymeric Endoluminal Paving. A Family of Evolving Methods for Extending Endoluminal Therapeutics beyond Stenting. Cardiol. Clin 1994, 12 (4), 715–737. [PubMed: 7850840]

(10). Ashton JH; Mertz JAM; Harper JL; Slepian MJ; Mills JL; McGrath DV; Vande Geest JP Polymeric Endoaortic Paving: Mechanical, Thermoforming, and Degradation Properties of Polycaprolactone/Polyurethane Blends for Cardiovascular Applications. Acta Biomater. 2011, 7 (1), 287–294. [PubMed: 20832506]

(11). Baikoussis NG; Antonopoulos CN; Papakonstantinou NA; Argiriou M; Geroulakos G. Endovascular Stent Grafting for Ascending Aorta Diseases. J. Vasc. Surg 2017, 66 (5), 1587–1601. [PubMed: 28830707]

(12). Agarwal S; High KM Newer-Generation Ventricular Assist Devices. Best Pract. Res. Clin. Anaesthesiol 2012, 26 (2), 117–130. [PubMed: 22910085]

(13). Rotman OM; Kovarovic B; Chiu W-C; Bianchi M; Marom G; Slepian MJ; Bluestein D. Novel Polymeric Valve for Transcatheter Aortic Valve Replacement Applications: In Vitro Hemodynamic Study. Ann. Biomed. Eng 2019, 47 (1), 113–125. [PubMed: 30194551]

(14). Slepian MJ; Alemu Y; Soares JS; Smith G., R.; Einav, S. The SyncardiaTM Total Artificial Heart: In Vivo, in Vitro, and Computational Modeling Studies. J. Biomech 2013, 46 (2), 266–275. [PubMed: 23305813]

(15). Orsello CE; Lauffenburger DA; Hammer DA Molecular Properties in Cell Adhesion: A Physical and Engineering Perspective. Trends Biotechnol. 2001, 19 (8), 310–316. [PubMed: 11451473]

(16). Dilley RJ; McGeachie JK; Prendergast FJ A Review of the Proliferative Behaviour, Morphology and Phenotypes of Vascular Smooth Muscle. Atherosclerosis 1987, 63 (2), 99–107. [PubMed: 3548737]

(17). Slepian MJ; Massia SP; Dehdashti B; Fritz A; Whitesell L. β 3 -Integrins Rather Than β 1 -Integrins Dominate Integrin-Matrix Interactions Involved in Postinjury Smooth Muscle Cell Migration. Circulation 1998, 97 (18), 1818–1827. [PubMed: 9603537]

(18). Wang D; Uhrin P; Mocan A; Waltenberger B; Breuss JM; Tewari D; Mihaly-Bison J; Huminiecki Ł; Starzy ski RR; Tzvetkov NT; et al. Vascular Smooth Muscle Cell Proliferation as a Therapeutic Target. Part 1: Molecular Targets and Pathways. Biotechnol. Adv 2018, 36 (6), 1586–1607. [PubMed: 29684502]

(19). Peyton SR; Putnam AJ Extracellular Matrix Rigidity Governs Smooth Muscle Cell Motility in a Biphasic Fashion. J. Cell. Physiol 2005, 204 (1), 198–209. [PubMed: 15669099]

(20). Nadia Zaari B; Rajagopalan P; Kim SK; Engler AJ; Wong JY; Wong JY; Zaari N; Rajagopalan P; Kim SK; Engler AJ Photopolymerization in Microfluidic Gradient Generators: Microscale Control of Substrate Compliance to Manipulate Cell Response**. Adv. Mater 2004, 16 (23±24), 2133–2137.

(21). Apoptotic Vascular Endothelial Cells Become Procoagulant: Bombeli T, Karsan A, Tait JF, Harlan JM. Blood 89:2429–2442, 1997 Transfus. Med. Rev. 1997, 11 (4), 314–315. [PubMed: 9116287]

(22). Bochenek ML; Schütz E; Schäfer K. Endothelial Cell Senescence and Thrombosis: Ageing Clots. Thromb. Res 2016, 147, 36–45. [PubMed: 27669126]

(23). Jia G; Aroor AR; Jia C; Sowers JR Endothelial Cell Senescence in Aging-Related Vascular Dysfunction. Biochim. Biophys. Acta - Mol. Basis Dis 2018.

(24). Nuzzolo ER; Iachininoto MG; Teofili L. Endothelial Progenitor Cells and Thrombosis. Thromb. Res 2012, 129 (3), 309–313. [PubMed: 22236662]

(25). Cox TR; Erler JT Remodeling and Homeostasis of the Extracellular Matrix: Implications for Fibrotic Diseases and Cancer. Dis. Model. Mech 2011, 4 (2), 165–178. [PubMed: 21324931]

(26). Mason BN; Starchenko A; Williams RM; Bonassar LJ; Reinhart-King CA Tuning Three-Dimensional Collagen Matrix Stiffness Independently of Collagen Concentration Modulates Endothelial Cell Behavior. Acta Biomater. 2013, 9 (1), 4635–4644. [PubMed: 22902816]

(27). van Wachem PB; Beugeling T; Feijen J; Bantjes A; Detmers JP; van Aken WG Interaction of Cultured Human Endothelial Cells with Polymeric Surfaces of Different Wettabilities. Biomaterials 1985, 6 (6), 403–408. [PubMed: 4084642]

(28). Cimmino G; Golino P. Platelet Biology and Receptor Pathways. J. Cardiovasc. Transl. Res 2013, 6 (3), 299–309. [PubMed: 23307175]

(29). Hasebe T; Ishimaru T; Kamijo A; Yoshimoto Y; Yoshimura T; Yohena S; Kodama H; Hotta A; Takahashi K; Suzuki T. Effects of Surface Roughness on Anti-Thrombogenicity of Diamond-like Carbon Films. Diam. Relat. Mater 2007, 16 (4–7), 1343–1348.

(30). Lee JH; Lee HB Platelet Adhesion onto Wettability Gradient Surfaces in the Absence and Presence of Plasma Proteins. J. Biomed. Mater. Res 1998, 41 (2), 304–311. [PubMed: 9638536]

(31). Skoog SA; Kumar G; Narayan RJ; Goering PL Biological Responses to Immobilized Microscale and Nanoscale Surface Topographies. Pharmacol. Ther 2017, 182, 33–55. [PubMed: 28720431]

(32). Gadelmawla ES; Koura MM; Maksoud TMA; Elewa IM; Soliman HH Roughness Parameters.

(33). Huhtamäki T; Tian X; Korhonen JT; Ras RH A. Surface-Wetting Characterization Using Contact-Angle Measurements. Nat. Protoc 2018, 13 (7), 1521–1538. [PubMed: 29988109]

(34). Ling Y. Uniaxial True Stress-Strain after Necking - Tyco Electronics; 2004.

(35). Jesty J; Bluestein D. Acetylated Prothrombin as a Substrate in the Measurement of the Procoagulant Activity of Platelets: Elimination of the Feedback Activation of Platelets by Thrombin. Anal. Biochem 1999, 272 (1), 64–70. [PubMed: 10405294]

(36). Fernández J; Auzmendi O; Amestoy H; Diez-Torre A; Sarasua J-R Mechanical Properties and Fatigue Analysis on Poly(ɛ-Caprolactone)-Polydopamine-Coated Nanofibers and Poly(ɛ-Caprolactone)-Carbon Nanotube Composite Scaffolds. Eur. Polym. J 2017, 94, 208–221.

(37). Cipolla M. The Vascular Smooth Muscle Cell: Molecular and Biological Responses to the Extracellular Matrix. J. Vasc. Surg 1997, 25 (3), 595.

(38). Lim JY; Donahue HJ Cell Sensing and Response to Micro- and Nanostructured Surfaces Produced by Chemical and Topographic Patterning. Tissue Eng 2007, 13 (8), 1879–1891. [PubMed: 17583997]

(39). Iivanainen E; Kähäri V-M; Heino J; Elenius K. Endothelial Cell–Matrix Interactions. Microsc. Res. Tech 2003, 60 (1), 13–22. [PubMed: 12500256]

(40). Ammann KR; DeCook KJ; Tran PL; Merkle VM; Wong PK; Slepian MJ Collective Cell Migration of Smooth Muscle and Endothelial Cells: Impact of Injury versus Non-Injury Stimuli. J. Biol. Eng 2015, 9, 19. [PubMed: 26473009]

(41). Hauser S; Jung F; Pietzsch J. Human Endothelial Cell Models in Biomaterial Research. 2017, 35 (3), 265–277.

(42). Cortina JM Interaction, Nonlinearity, and Multicollinearity: Implications for Mu/Tip/e Regression; 1993; Vol. 19.

(43). Mason CH; Perreault WD Collinearity, Power, and Interpretation of Multiple Regression Analysis. J. Mark. Res 1991, 28 (3), 268.

(44). Webb HK; Truong VK; Hasan J; Fluke C; Crawford RJ; Ivanova EP Roughness Parameters for Standard Description of Surface Nanoarchitecture. Scanning 2012, 34, 257–263. [PubMed: 22331659]

(45). Suh AY; Polycarpou AA; Conry TF Detailed Surface Roughness Characterization of Engineering Surfaces Undergoing Tribological Testing Leading to Scuffing. Wear 2003, 255 (1–6), 556–568.

(46). Järnström J; Ihalainen P; Backfolk K; Peltonen J. Roughness of Pigment Coatings and Its Influence on Gloss. Appl. Surf. Sci 2008, 254 (18), 5741–5749.

(47). Méndez-Vilas A; Bruque JM; González-Martín ML Sensitivity of Surface Roughness Parameters to Changes in the Density of Scanning Points in Multi-Scale AFM Studies. Application to a Biomaterial Surface. Ultramicroscopy 2007, 107 (8), 617–625. [PubMed: 17292550]

(48). Lamolle SF; Monjo M; Lyngstadaas SP; Ellingsen JE; Haugen HJ Titanium Implant Surface Modification by Cathodic Reduction in Hydrofluoric Acid: Surface Characterization and in Vivo Performance. J. Biomed. Mater. Res. Part A 2009, 88A (3), 581–588.

(49). Andrukhov O; Huber R; Shi B; Berner S; Rausch-Fan X; Moritz A; Spencer ND; Schedle A. Proliferation, Behavior, and Differentiation of Osteoblasts on Surfaces of Different Microroughness. Dent. Mater 2016, 32 (11), 1374–1384. [PubMed: 27637551]

(50). Rosales-Leal JI; Rodríguez-Valverde MA; Mazzaglia G; Ramón-Torregrosa PJ; Díaz-Rodríguez L; García-Martínez O; Vallecillo-Capilla M; Ruiz C; Cabrerizo-Vílchez MA Effect of Roughness, Wettability and Morphology of Engineered Titanium Surfaces on Osteoblast-like Cell Adhesion. Colloids Surfaces A Physicochem. Eng. Asp 2010, 365 (1–3), 222–229.

(51). Brown CA; Hansen HN; Jiang XJ; Blateyron F; Berglund J; Senin N; Bartkowiak T; Dixon B; Le Goïc G; Quinsat Y; et al. Multiscale Analyses and Characterizations of Surface Topographies. CIRP Ann. 2018, 67 (2), 839–862.

(52). Vadillo-Rodríguez V; Guerra-García-Mora AI; Perera-Costa D; Gónzalez-Martín ML; Fernández-Calderón MC Bacterial Response to Spatially Organized Microtopographic Surface Patterns with Nanometer Scale Roughness. Colloids Surfaces B Biointerfaces 2018, 169, 340–347. [PubMed: 29800909]

(53). Tripathy A; Kumar A; Sreedharan S; Muralidharan G; Pramanik A; Nandi D; Sen P. Fabrication of Low-Cost Flexible Superhydrophobic Antibacterial Surface with Dual-Scale Roughness. ACS Biomater. Sci. Eng 2018, 4 (6), 2213–2223.

(54). Strohbach A; Busch R. Polymers for Cardiovascular Stent Coatings. Int. J. Polym. Sci 2015, 2015, 1–11.

(55). Chiono V; Mozetic P; Boffito M; Sartori S; Gioffredi E; Silvestri A; Rainer A; Giannitelli SM; Trombetta M; Nurzynska D; et al. Polyurethane-Based Scaffolds for Myocardial Tissue Engineering. Interface Focus 2014, 4 (1), 20130045.

(56). Henry BJ; Carlin JP; Hammerschmidt JA; Buck RC; Buxton LW; Fiedler H; Seed J; Hernandez O. A Critical Review of the Application of Polymer of Low Concern and Regulatory Criteria to Fluoropolymers. Integr. Environ. Assess. Manag 2018, 14 (3), 316–334. [PubMed: 29424474]
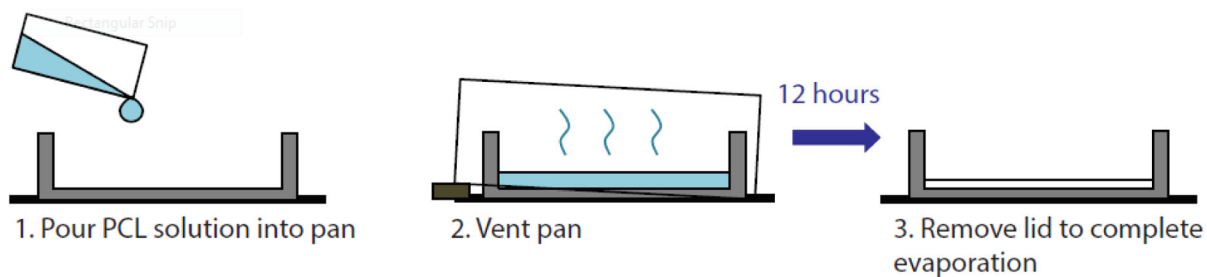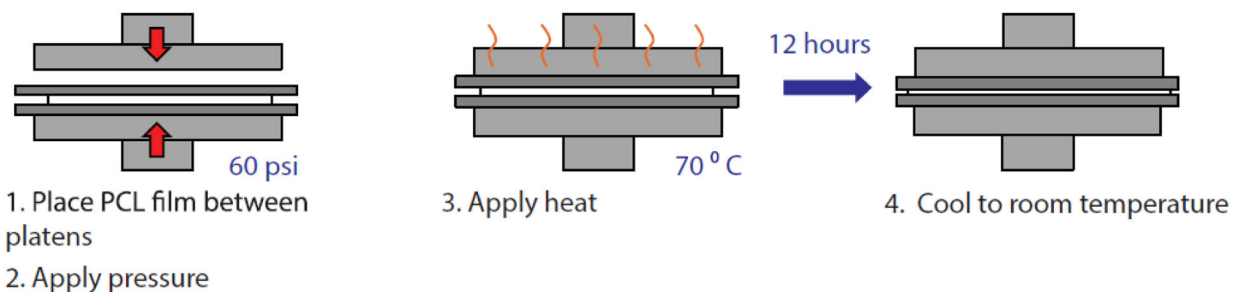
A Solvent Cast

1. Pour PCL solution into pan

2. Vent pan

12 hours

3. Remove lid to complete evaporation

B Melt Press

60 psi

1. Place PCL film between platens
2. Apply pressure

3. Apply heat

70 °C

12 hours

4. Cool to room temperature

C Spin Coat

1. Pour PCL solution onto glass slide mounted to spin-coater chuck

2. Spin chuck

1500 RPM

3. Repeat once for desired thickness
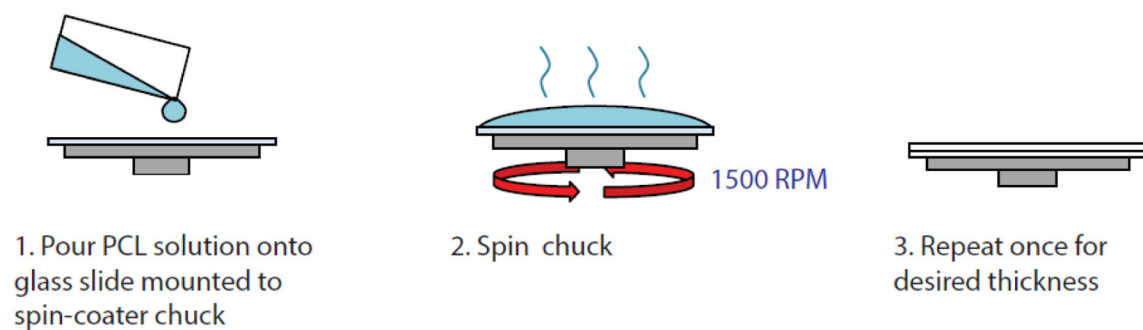
Figure 1. PCL Film Formation Methods.
Brief description of protocol to form uniform PCL films via solvent cast (A), melt press (B), and spin coat (C) techniques.
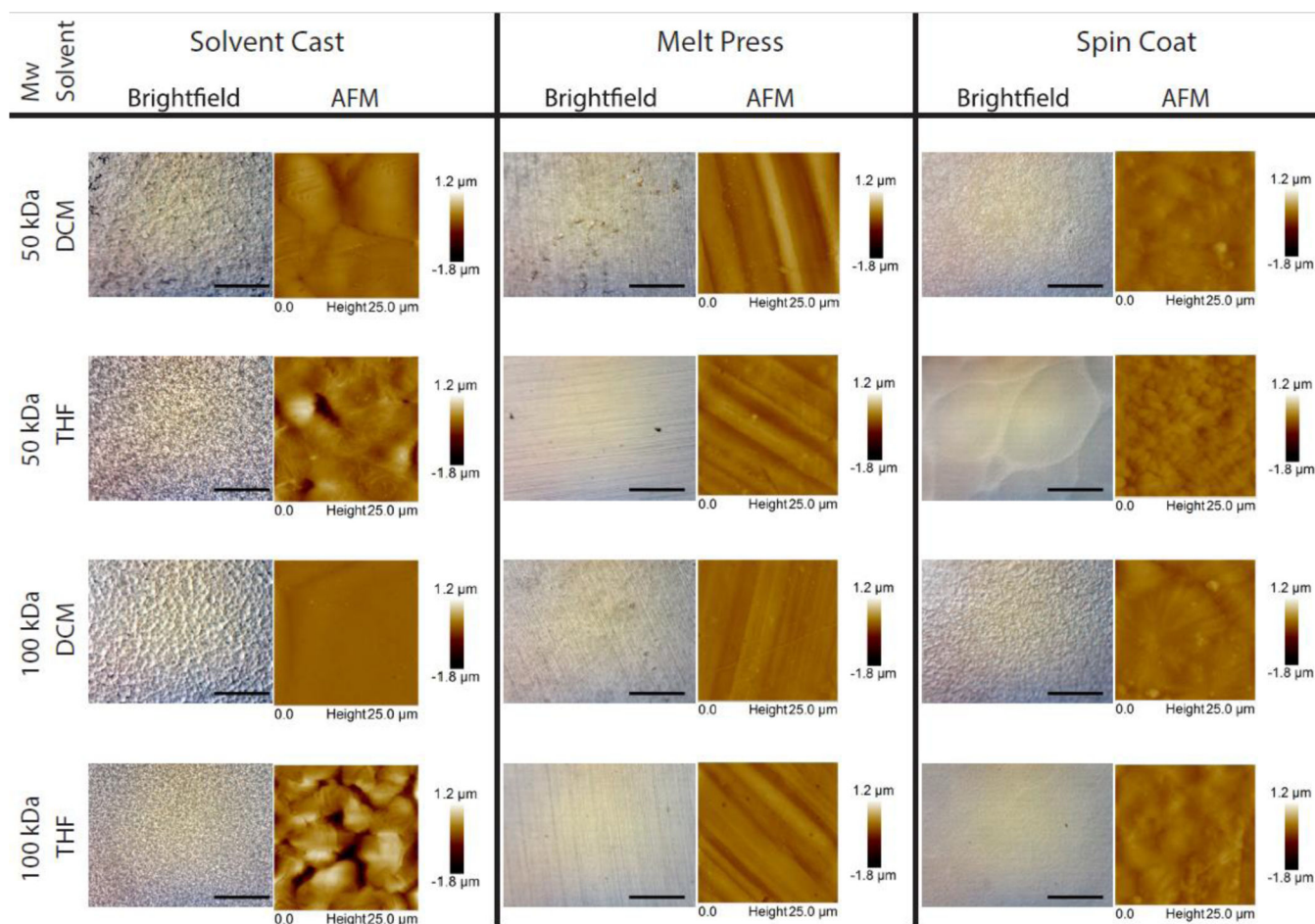
Figure 2. Images of Twelve Uniquely Formed PCL Films.

Each column depicts microscope brightfield images (left) and AFM 2-dimensional surface topographic images (right) of three film formation methods: solvent cast (left), melt press (middle) and spin coat (right). Each row is divided into the different molecular weights used to form the PCL: 50 kDa (top two rows) and 100 kDa (bottom two rows). Rows are further separated by alternating solvents used to dissolve and form PCL film: dichloromethane and tetrahydrofuran. Brightfield scale bars are depicted in bottom right of each image and represent 1 mm. AFM images represent a 25.0 μm x 25.0 μm section of the PCL film, legends to right of image correspond to height of topographic features between −1.8 μm and 1.2 μm.
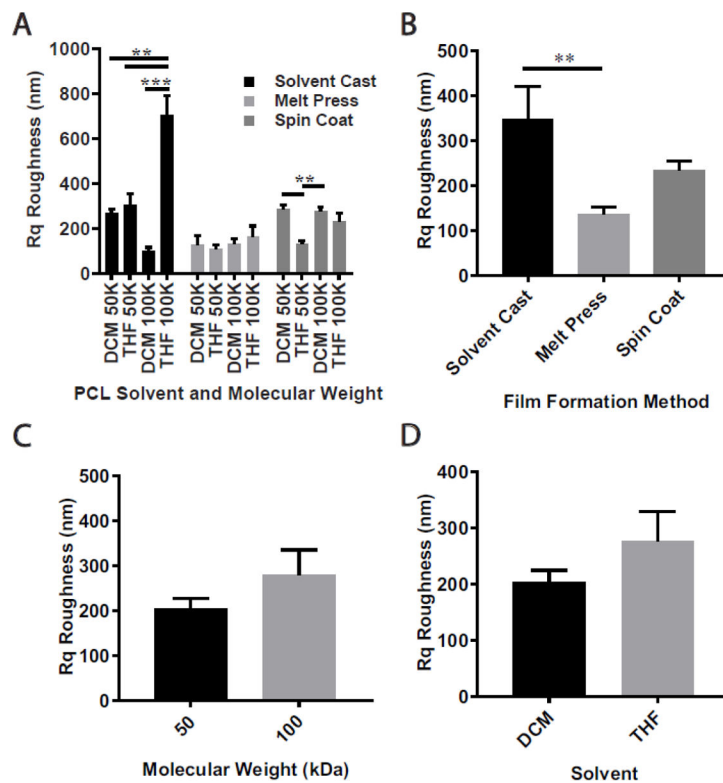
Figure 3. Roughness of PCL Films.

Root-mean-square topographic heights (Rq) of each individual film was measured to obtain roughness (A). Roughness was compared between varying film formation method (B), molecular weight (C) and solvent (D). ** denotes significant difference with $p < 0.01$; *** denotes significant difference with $p < 0.005$. Values are displayed as mean roughness (n ≥ 3) ± standard error.
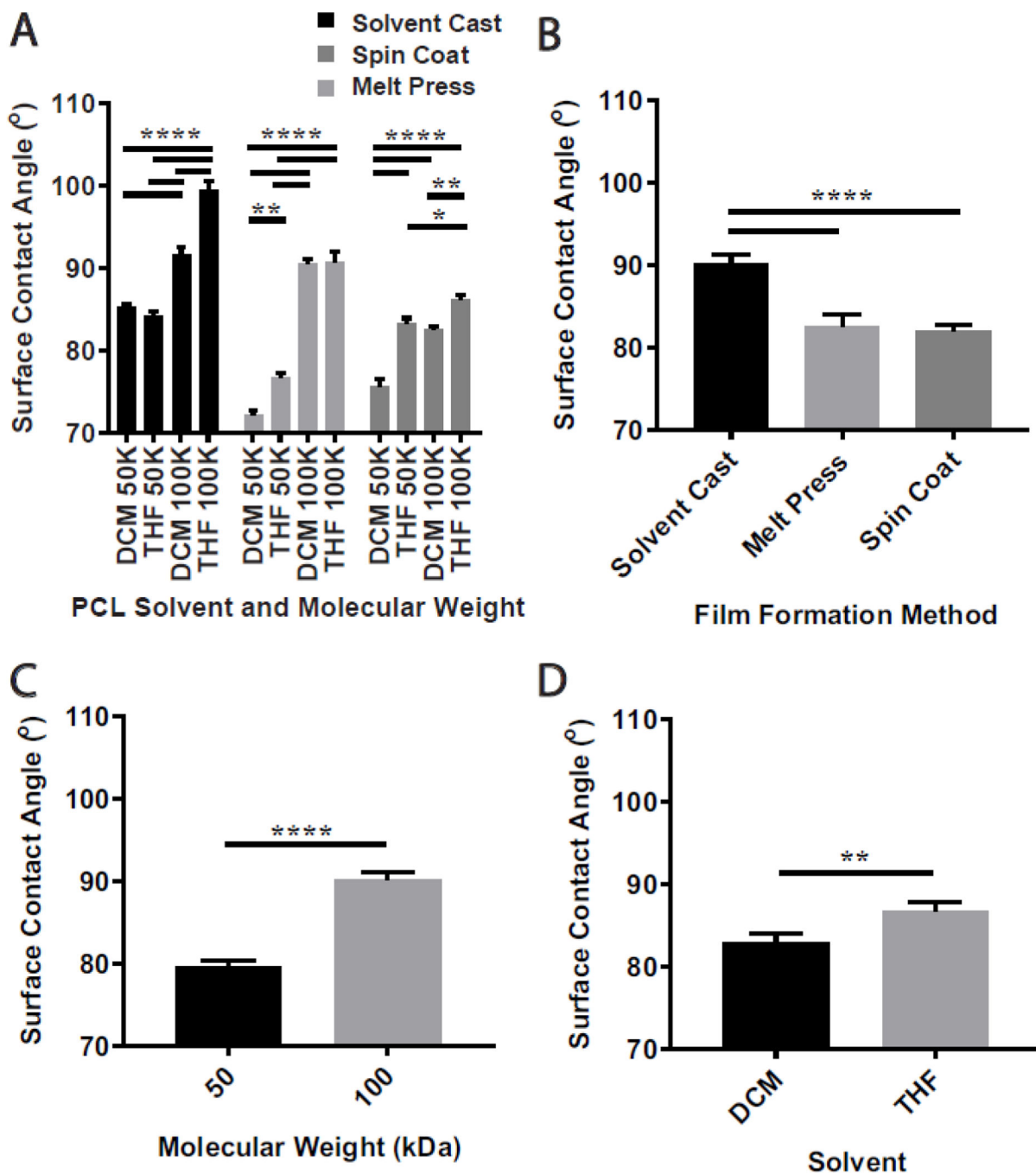
Figure 4. Wettability of PCL Films.
Surface contact angle (°) of each individual film was measured to obtain wettability; contact angle has inverse relationship to wettability (A). Wettability was compared between varying film formation method (B), molecular weight (C) and solvent (D). * denotes significant difference with $p < 0.05$; ** denotes significant difference with $p < 0.01$; **** denotes significant difference with $p < 0.001$. Values are displayed as mean wettability (n ≥ 3) ± standard error.
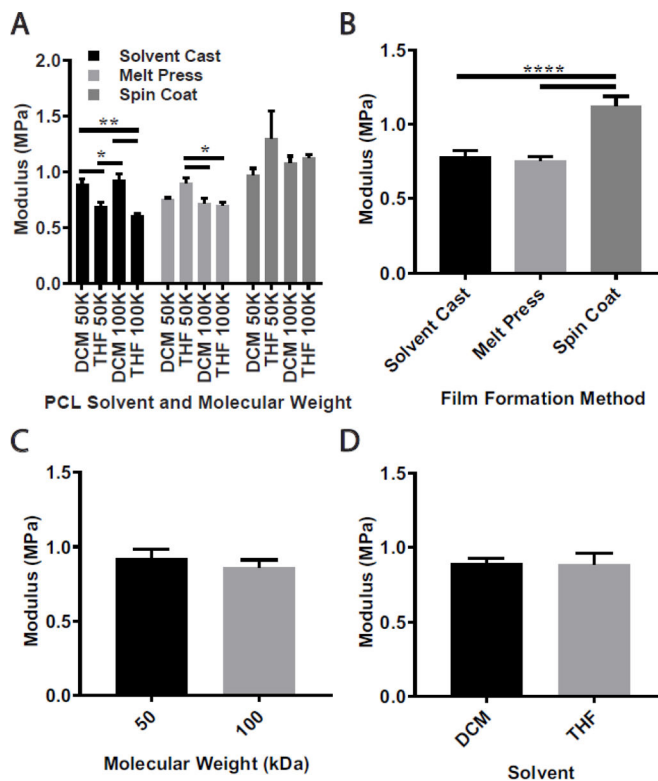
Figure 5. Stiffness of PCL Films.

Young's modulus (MPa) of each individual film was measured to obtain bulk stiffness (A). Stiffness was compared between varying film formation method (B), molecular weight (C) and solvent (D). * denotes significant difference with $p < 0.05$; ** denotes significant difference with $p < 0.01$; **** denotes significant difference with $p < 0.001$. Values are displayed as mean stiffness (n ≥ 3) ± standard error.
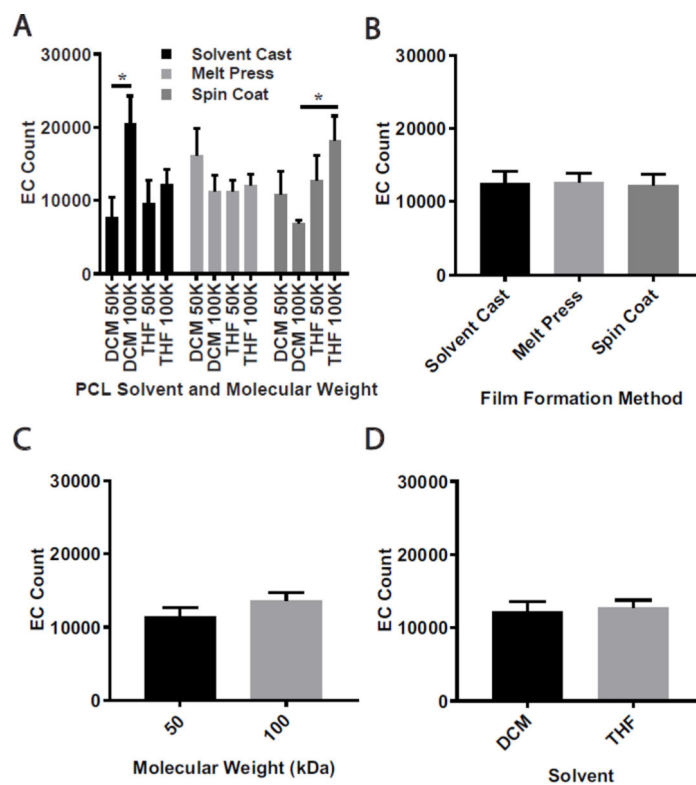
Figure 6. EC Adhesion to PCL Films.

EC count after 24 hours incubation with each individual film was measured via fluorescence to obtain EC adhesion (A). EC adhesion was compared between varying film formation method (B), molecular weight (C) and solvent (D). * denotes significant difference with $p < 0.05$. Values are displayed as mean EC count (n ≥ 9) ± standard error.
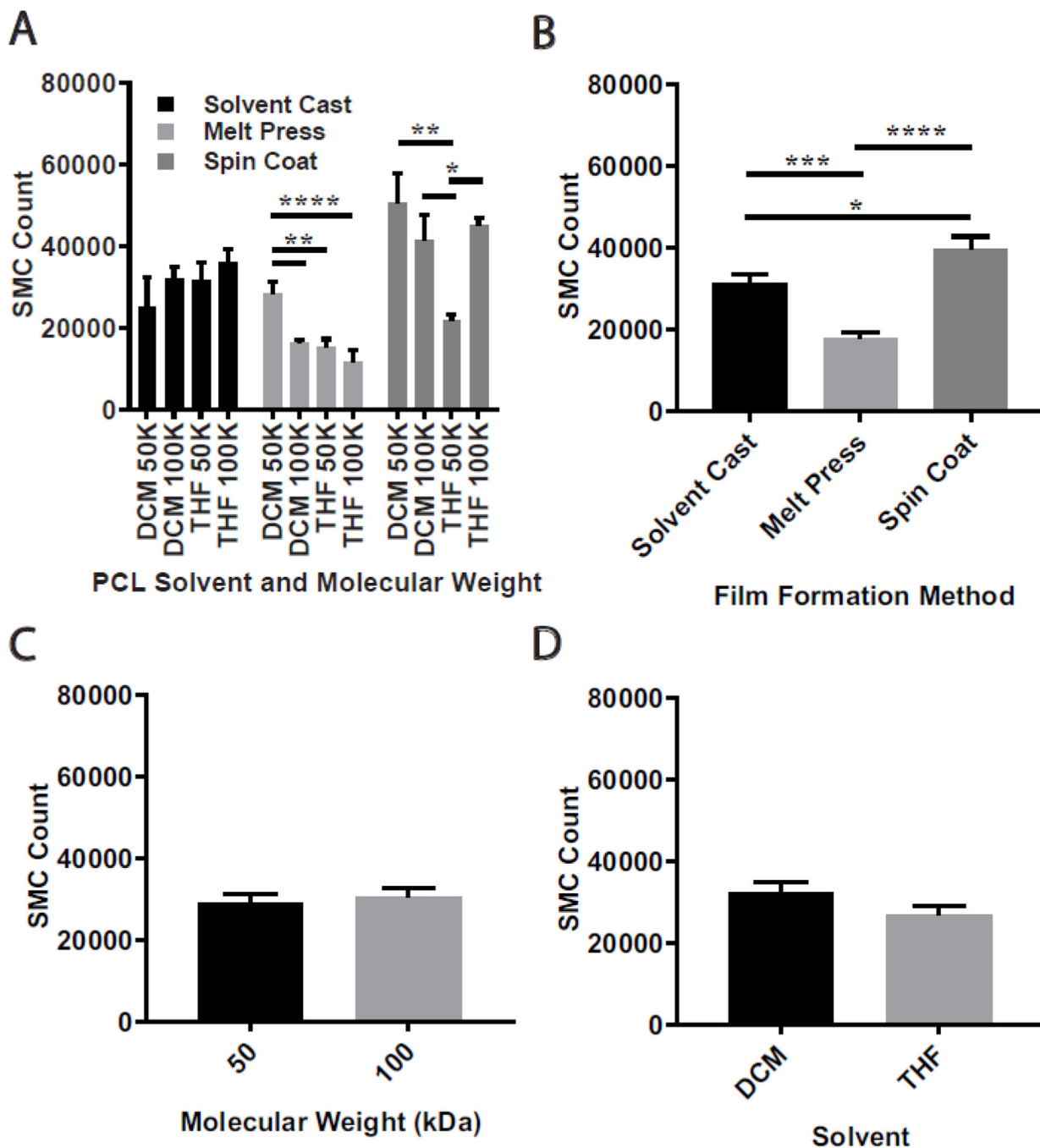
Figure 7. SMC Adhesion to PCL Films.
SMC count after 24 hours incubation with each individual film was measured via fluorescence to obtain SMC adhesion (A). SMC adhesion was compared between varying film formation method (B), molecular weight (C) and solvent (D). * denotes significant difference with $p < 0.05$; ** denotes significant difference with $p < 0.01$; *** denotes significant difference with $p < 0.005$; **** denotes significant difference with $p < 0.001$. Values are displayed as mean SMC count (n ≥ 9) ± standard error.
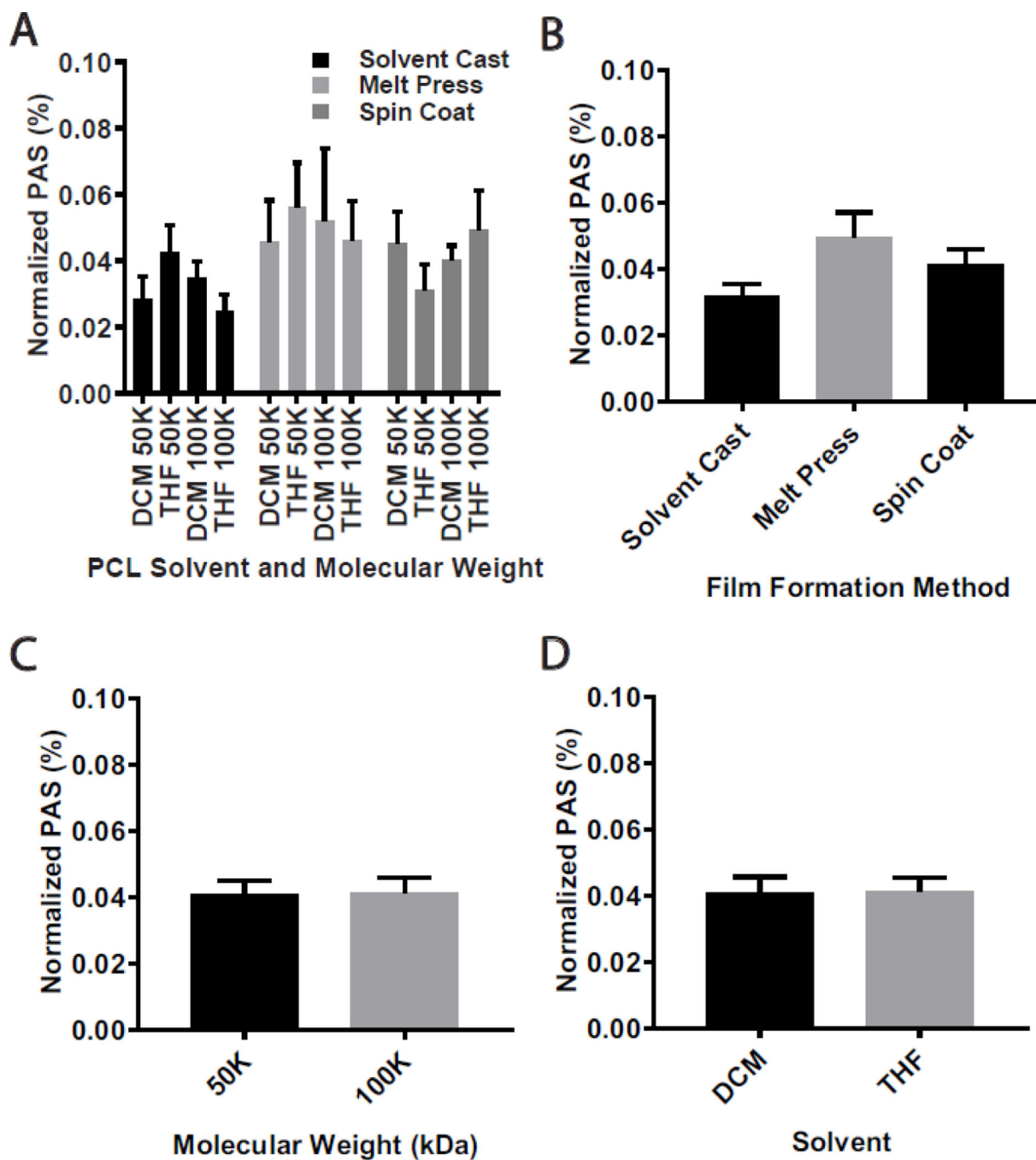
Figure 8. Platelet Activation Response to PCL Films.
Thrombin generation rate after 30 minutes incubation with each individual film was measured to obtain PAS (A). PAS was compared between varying film formation method (B), molecular weight (C) and solvent (D). Values are displayed as mean PAS (n ≥ 9) ± standard error.

Table 1.

Multiple Regression Analysis - Effect Summary of Polymer Processing Methods on Physical Characteristics

Dependent Variable	Model Fit F-Ratio	Model Fit P-Value	Independent Variables	P-Value	Parameter Estimate
Roughness (R_q)	0.94	0.49	Film Formation Method	0.32	Solvent Cast: 90.84 Melt Press: −81.74 Spin Coat: −9.09
			Solvent	0.37	DCM: −41.6 THF: 41.6
			Molecular Weight	0.17	50 kDa: −18.64 100 kDa: 18.64
Wettability (°)	*9.88*	*0.005*	Molecular Weight	*0.002*	50 kDa: −5.31 100 kDa: 5.31
			Film Formation Method	*0.03*	Solvent Cast: 5.27 Melt Press: −2.34 Spin Coat: −2.93
			Solvent	0.12	DCM: −1.9 THF: 1.9
Stiffness (MPa)	*4.21*	*0.05*	Film Formation Method	*0.02*	Solvent Cast: −0.10 Melt Press: −0.15 Spin Coat: 0.25
			Solvent	0.72	DCM: 0.02 THF: −0.02
			Molecular Weight	0.77	50 kDa: 0.01 100 kDa: −0.01

Table 2.

Multiple Regression Analysis - Effect Summary of Polymer Physical Characteristics on Cell and Polymer Surface Interaction

Dependent Variable	Model Fit F-Ratio	Model Fit P-Value	Independent Variables	P-Value	Parameter Estimate
EC Adhesion (EC Count)	0.62	0.62	Wettability (°)	0.35	−209.48
			Stiffness (MPa)	0.37	−6924.62
			Roughness (R_q)	0.65	5.12
SMC Adhesion (SMC Count)	*4.13*	*0.05*	Roughness (R_q)	*0.03*	57.82
			Stiffness (MPa)	*0.04*	36901.30
			Wettability (°)	0.22	−542.29
PAS (%)	1.09	0.42	Roughness (R_q)	0.25	−2.87E-5
			Stiffness (MPa)	0.40	−0.00035
			Wettability (°)	0.46	−0.014

Table 3.

Multiple Regression Analysis - Effect Summary of Polymer Processing Methods on Cell and Polymer Surface Interaction

Dependent Variable	Model Fit F-Ratio	Model Fit P-Value	Independent Variables	P-Value	Parameter Estimate
EC Adhesion (EC Count)	0.16	0.95	Solvent	0.47	DCM: −1071.03 THF: 1071.03
			Molecular Weight	0.87	50 kDa: −237.07 100 kDa: 237.07
			Film Formation Method	0.99	Solvent Cast: 37.29 Melt Press: 211.12 Spin Coat: −248.41
SMC Adhesion (SMC Count)	*3.15*	*0.09*	Film Formation Method	*0.03*	Solvent Cast: 1588.17 Melt Press: −11746.64 Spin Coat: 10158.47
			Molecular Weight	0.35	50 kDa: 2650.52 100 kDa: −2650.52
			Solvent	0.17	DCM: −848.54 THF: 848.54
PAS (%)	*5.30*	*0.05*	Film Formation Method	*0.02*	Solvent Cast: −0.011 Melt Press: 0.008 Spin Coat: 0.003
			Molecular Weight	0.20	50 kDa: −0.003 100 kDa: 0.003
			Solvent	0.21	DCM: 0.003 THF: −0.003